Available online at www.sciencedirect.com

ScienceDirect

Procedia Structural Integrity 33 (2021) 1065–1072

Structural Integrity Procedia

www.elsevier.com/locate/procedia

IGF26 - 26th International Conference on Fracture and Structural Integrity

Finding the optimal stress state of a stainless-steel IPE profile for fatigue experiments

Lucas Braet[a], Tereza Juhászová [b,c], Daniel Jindra[c], Petr Miarka [b,c]*, Stanislav Seitl[b,c]

[a]*Ghent University, Faculty of Engineering and Architecture, Jozef Plateaustraat 22 , Gent 9000, Belgium*
[b]*Institute of Physics of Materials, Czech Academy of Sciences, Žižkova 22, Brno 616 62, Czech Republic*
[bc] *Faculty of Civil Engineering, Brno University of Technology, Veveří 331/95, Brno 602 00, Czech Republic*

Abstract

Pilot fatigue experiments of a stainless-steel IPE80 profile showed local bending at the top flange and a global stability loss. Therefore, in this paper we present a non-linear numerical study of such profile to achieve an optimal stress state and reduce the possible stability loss and to keep the stress distribution close to Euler-Bernoulli's beam theory. This was assessed by reaching a tensile stress in the bottom flange less than the material's yielding strength and by a varying span to the profile's height and by varying the loading options from three-point bending to four-point bending.

Keywords: IPE profile; stainless steel; FEM; fatigue;

1. Introduction

Owing to its unique combination of excellent corrosion resistance, durability, attractive appearance and favorable mechanical properties, stainless steel is increasingly being used in the construction industry. According to cost-efficiency studies, the usage of certain stainless steel is the most beneficial in cases of bridges exposed to aggressive environmental conditions with heavy traffic volumes. It is possible to assess the cost efficiency through life cycle cost (LCC) analyses when used in bridge construction Daghash (2019). The difference between construction steel and

* Corresponding author. Tel.: +420-532-290-361.
E-mail address: miarka@imp.cz

10.1016/j.prostr.2021.10.118

stainless steel is primarily the difference in price (stainless steel is more expensive than construction steel). Another difference is the

Nomenclature

ε	strain (-)
δ	vertical diplacement
σ	stress (MPa)
$\sigma_{0.2}$	0.2 % proof stress (MPa)
u_z	displament in Z-axis
E	Young's modulus (GPa)
S	profile's span (mm)
H	profile's height (mm)

deformation of construction steel before failure (see difference in stress-strain curves), in this way it gives a warning about the impending danger of failure. The last difference is the excellent corrosion resistance of stainless steel compared to construction steel.

Fig. 1: Failed fatigue experiment of IPE80 profile – right buckling – left plastic deformation under the load.

The buckling analysis of stainless-steel IPE80 profile was done by Jindra et al. (2020) and Jindra et al. (2021). In this contribution we aim to analyse the various span lengths of IPE 80 profile in two loading case – three and four point bending in order pro find optimum stress state for which a fatigue testing will be possible.

2. Material

This numerical study is based on the experimental test of the IPE 80 profile made of stainless-steel grade EN 1.4301 / AISI 304. The material properties and chemical composition as presented here is based on the inspection certificate (attest of Montanstahl AG, certificate no. 127381-00, in accordance with EN 10204 3.1, size standard EN 10034, product standard EN 10365). The material's chemical composition together with measured mechanical properties of two tested specimen are presented in Table 1.

Table 1. Chemical composition in percentage by weight (wt. %) and material properties of the stainless-steel specimens.

Specimen	C	Si	Mn	P	S	Ni	Cr	N	Tensile strength [MPa]	0.2 % proof stress [MPa]	1.0 % proof stress [MPa]	Elongation [%]
1	0.030	0.36	1.51	0.030	0.002	8.00	18.30	0.060	675	342	380	55
2	0.017	0.44	1.55	0.27	0.002	8.00	18.20	0.050	628	255	319	58

2.1. Material model

A suitable description of the stress-strain diagram of the stainless-steel material was proposed by Ramberg and Osgood(1943), later modified by Hill (1944):

$$\varepsilon = \frac{\sigma}{E_0} + 0.002\left(\frac{\sigma}{\sigma_{0.2}}\right)^n, \quad (1)$$

where σ and ε are the engineering stress and strain respectively, E_0 is the elastic Young's modulus, $\sigma_{0.2}$ is the material's 0.2% proof stress (the equivalent of the yield strength), and n states for a strain hardening exponent. The material behavior in accordance with this formulation results in a nice agreement with the experimental data of the stainless steel specimens for stress values up to the $\sigma_{0.2}$ value. However, according to the results of various studies, e.g. the one by Gardner (2001), at higher strains, the model overestimates the stress values. A compound two stage stress-strain curve devised by Mirambell and Real (2000) provides better agreement with the stress-strain experimental data for stress values above the 0.2% proof stress value in accordance with various studies, e.g. the one by Garden (2001). The second stage of this relation is defined as:

$$\varepsilon = \frac{\sigma-\sigma_{0.2}}{E_{0.2}} + \left(\varepsilon_{tu} - \frac{\sigma-\sigma_{0.2}}{E_{0.2}} - \varepsilon_{t0.2}\right)\left(\frac{\sigma-\sigma_{0.2}}{\sigma_u-\sigma_{0.2}}\right)^{n_{0.2,u}} + \varepsilon_{t0.2} \Leftrightarrow \sigma > \sigma_{0.2}, \quad (2)$$

where σ_u is the ultimate strength of the stainless steel, $n^{'0.2,u}$ is the strain hardening exponent, $\varepsilon_{t0.2}$ is the total strain at the 0.2% proof stress, ε_{tu} is the total strain at ultimate stress, and $E_{0.2}$ is the stiffness (tangent modulus) at the 0.2 % proof stress given as:

$$E_{0.2} = \frac{E}{1+0.002 \cdot n \cdot E_0/\sigma_{0.2}}, \quad (3)$$

A multi-linear material model with isotropic hardening (Von Mises plasticity) has been used for the numerical analysis as it is implemented in the FEM software Ansys. Using the mechanical parameters from tab. 1 into Eqs. (1)-(3) one can obtain following material curve which served as an input to FEM software for both tested specimens. The input material curves are showed in **Errore. L'origine riferimento non è stata trovata.**.

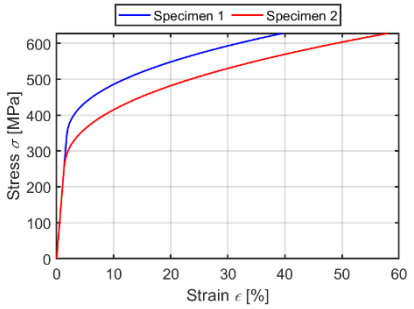

Fig. 2: Stress-strain material input as used in FEM software.

Together with data from tab. 1 exponents n and $n_{0.2,u}$ from Eq. (1) and (2) were for both specimens – 10.6 and 2.3, respectively.

3. Numerical model

In this numerical study, the geometry of an IPE80 profile was created in finite-element method (FEM) software ANSYS to obtain numerical results in reasonable time with sufficient accuracy. The numerical model was meshed with 3D 20-node solid elements SOLID186 with size of 2.5 mm. The model was refined in the top and bottom flange, while reducing the element number over the profile's span. The total number of elements is 6 000 with 30 000 nodes.

Since the given geometry allows to use an advantage of existing symmetry, only one-quarter of profile was modelled. The mesh and boundary conditions are showed in following figure.

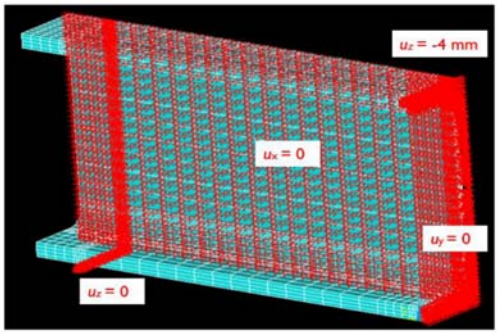

Fig. 3: Meshed IPE 80 profile with applied boundary conditions.

The numerical model was loaded with induced displacement of top support (placed in the mid-span of the profile) u_z = -4 mm and adequate boundary conditions were added to achieve the model's symmetry conditions and to prevent a rigid body rotation.

To analyze the stress distribution and find the optimum stress state, the IPE profile was loaded as a three-point bending (3PBT) and four-point bending test (4PBT). Furthermore, the ratio of span S to profile's height H varied. The studied ratios were S/H = 3; 4; 6; 8; and 10.

4. Numerical results

4.1. Model verification

In order to calibrate the numerical model, the material curve shown in **Errore. L'origine riferimento non è stata trovata.**, was used as an input for each specimen and the numerically generated force vs deformation (P-δ) results were compared with the experimentally measured curves. This comparison is shown in **Errore. L'origine riferimento non è stata trovata.**.

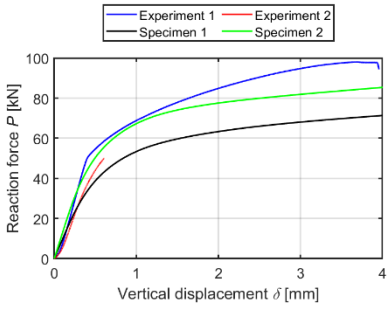

Fig. 4: Comparison of numerically generated force vs deformation diagram with experimentally measured curve.

From **Errore. L'origine riferimento non è stata trovata.** a relatively good agreement between the experimental and numerically generated P-δ curve can be observed. The input material curve as measured for specimen 1 shows a higher error to experiments, which is caused by the use of lower tensile strength of the material $\sigma_{0.2}$ of 255 MPa. On the other hand, the material input for the second specimen shows better agreement to experimental curves as it has a higher $\sigma_{0.2}$ of 355 MPa. Moreover, the second material curve (specimen 2) predicts the profile yielding more accurately

up to 1.5 mm of vertical displacement, as this is the limit in which the fatigue tests can be performed. Based on that, the second material curve will serve as an input for further numerical analysis.

4.2. Three-point bending

The numerically generated stress distributions in the IPE 80 profile are here under shown for various *S*/*H* ratios. The Von Mises stress distribution was selected for comparison as it provides relevant information about the material yielding due to the used material model. The Von Mises stresses in a 3PBT load case for a vertical deformation of u_z = 0.6 are shown in the following figure:

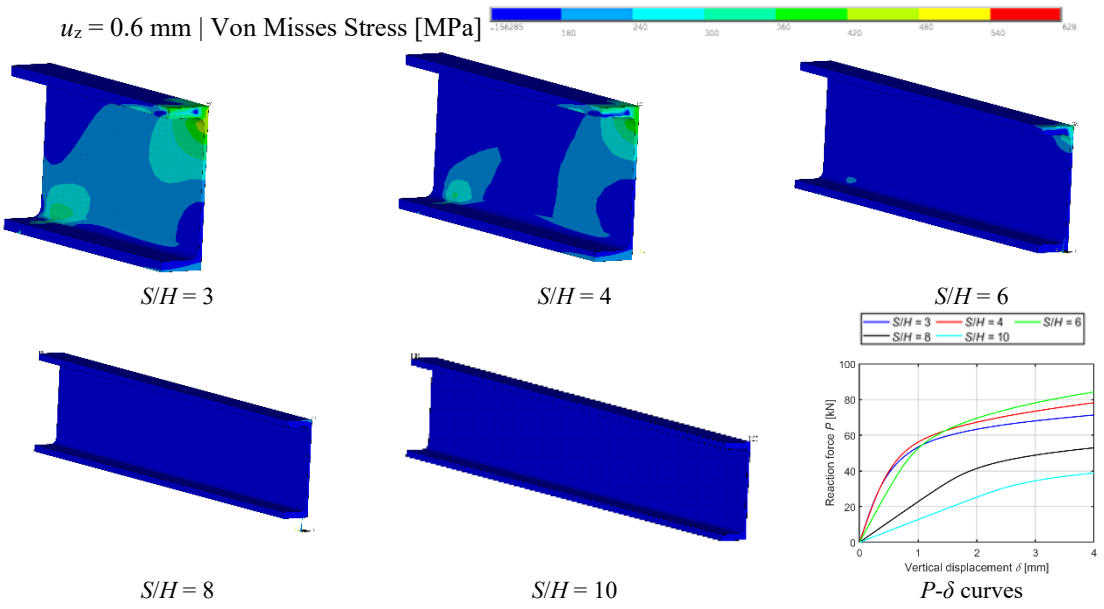

Fig. 5: Numerically generated Von Mises stress distribution for various *S*/*H* ratios for 3PBT load case.

The Von Mises stress in a 3PBT load case for a vertical deformation of u_z = 4 mm i.e. the testing machine limit, are presented in the following figure:

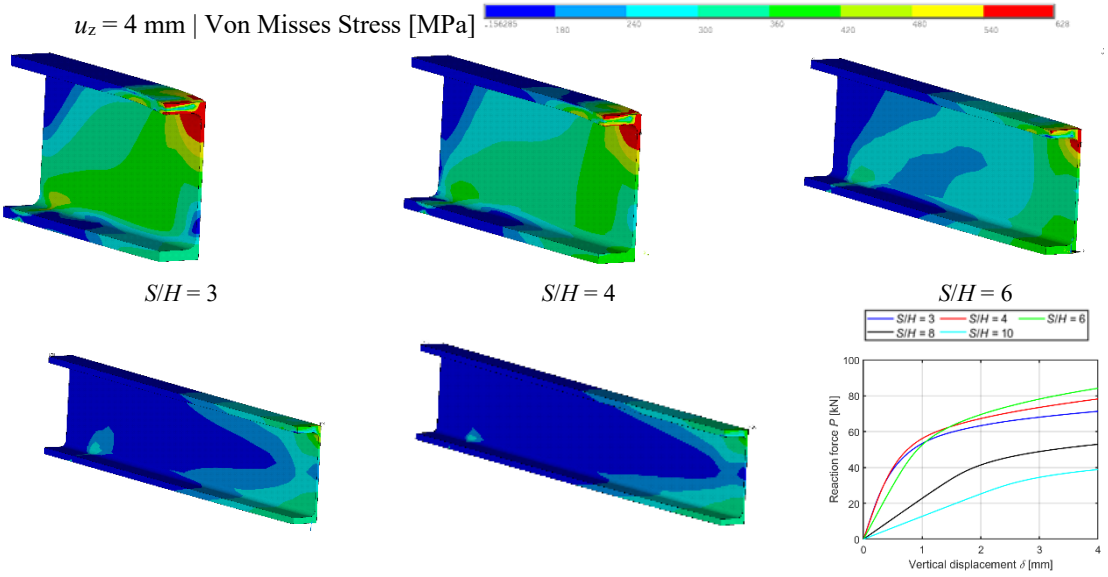

S/*H* = 8 *S*/*H* = 10 *P*-*δ* curves

Fig. 6: Numerically generated Von Mises stress distribution for various *S*/*H* ratios for 3PBT load case.

4.3. Four-point bending

By selecting the 4PBT loading, local material's yielding can be reduced and thus the higher force can be achieved by testing apparatus. The Von Mises stresses in the 4PBT load case for a vertical deformation of $u_z = 0.6$ are shown in the following figure:

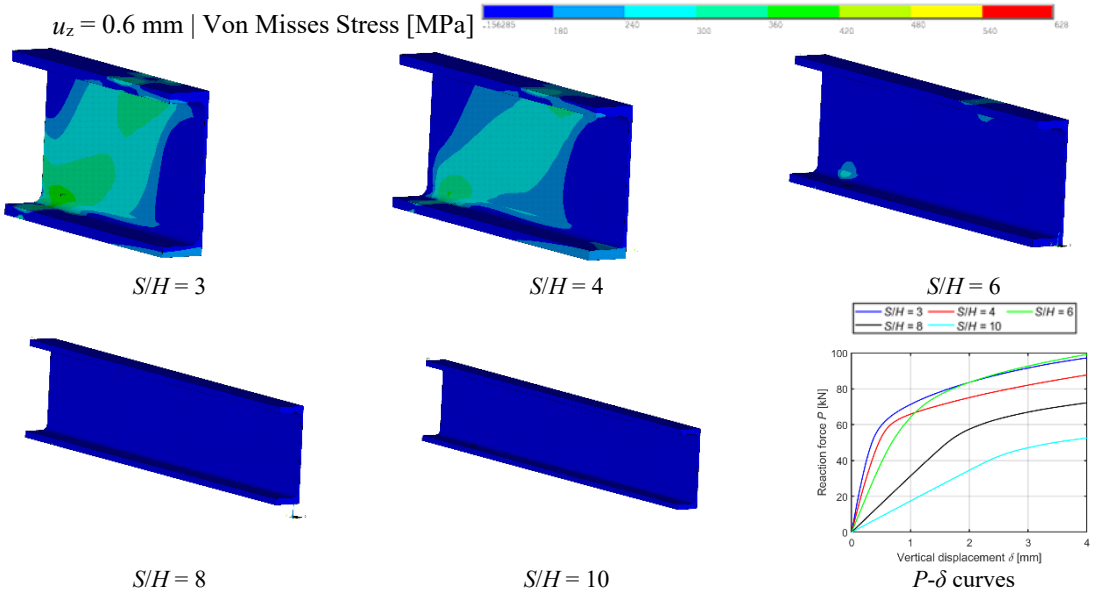

S/*H* = 8 *S*/*H* = 10 *P*-*δ* curves

Fig. 7: Numerically generated Von Mises stress distribution for various *S*/*H* ratios for 3PBT load case.

The Von Mises stress in a 3PBT load case with a vertical deformation of $u_z = 4$ mm i.e. the testing machine limit, are presented in the following figure:

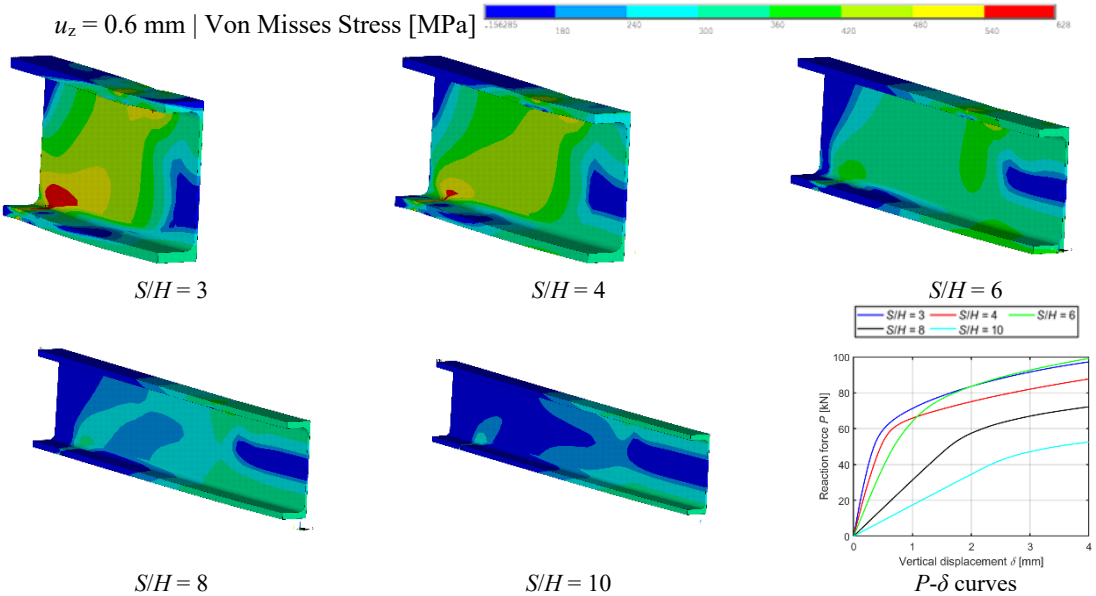

S/*H* = 8 *S*/*H* = 10 *P*-*δ* curves

Fig. 8: Numerically generated Von Mises stress distribution for various *S*/*H* ratios for 3PBT load case.

4.4. Stress in the profile

In order to directly compare the numerically generated stresses, the stress from S_{yy} and Von Mises were compared. The stress from Sy and the Von Mises stress were plotted in order to compare the numerically generated stresses. The stress for the comparison was taken from the path located in the middle of the specimen and is following the specimen's height. The stress comparison is shown in the following figures:

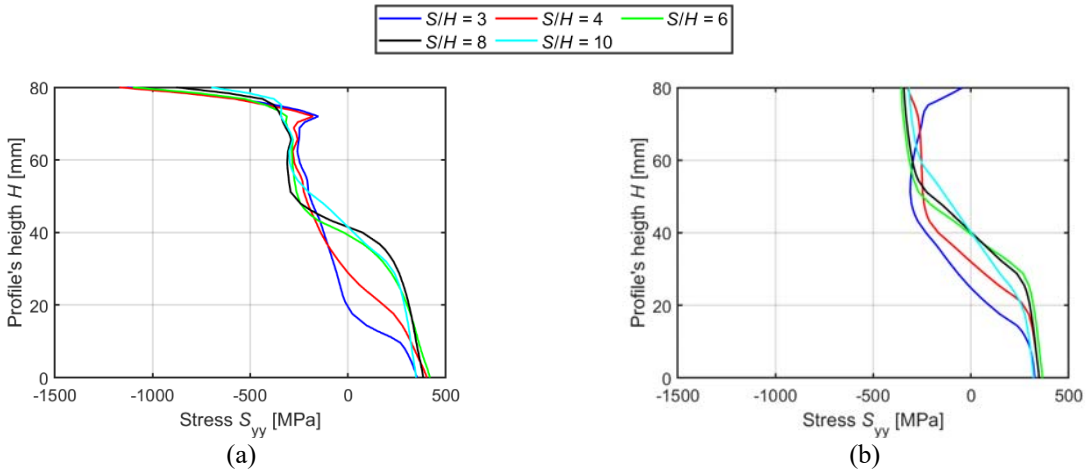

Fig. 9: Stress S_{yy} over the profile's height – (a) 3PBT and (b) 4PBT for studied *S*/*H* ratios.

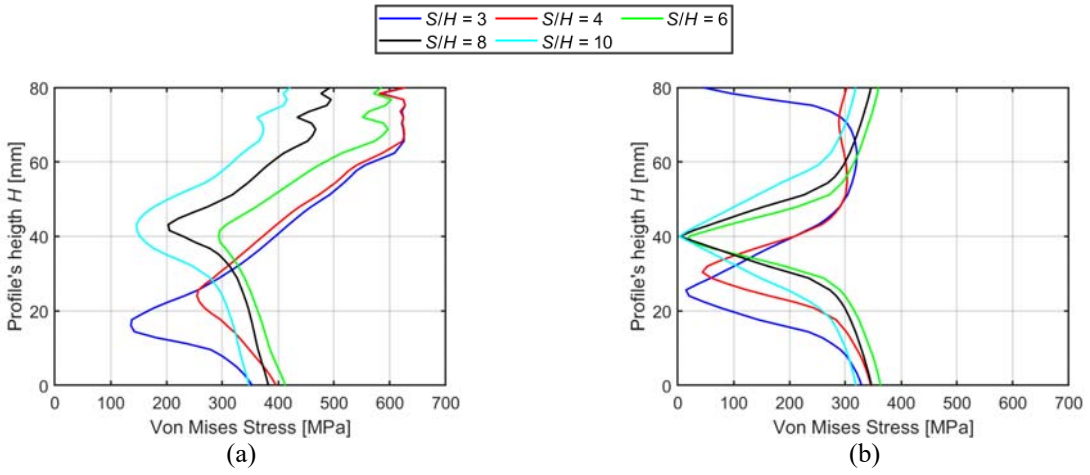

Fig. 10: Von Mises stress over the profile's height – (a) 3PBT and (b) 4PBT for studied *S*/*H* ratios.

From both Fig. 9 and Fig. 10 a clear reduction of stress in the profile for span ratio *S*/*H* bigger than 4. Furthermore, if the 4PBT is used the compressive stress in the top flange is reduced, which lowers the chance of buckling failure. For the 3PBT load case, the stress distribution close to Euler-Bernoulli is achieved for $S/H > 6$, while for the 4PBT case, this is achieved for $S/H = 4$. Thus, this suggest to be used in the future fatigue experiments, which the lower stresses are necessary.

5. Conclusion

In this numerical study a various S/H ratios of the stainless-steel IPE 80 profile were studied in two load case 3PBT and 4PBT. The numerical results showed, that if the span is increased, the stress in the profile is reduced together with the stress distribution is closed to Euler-Bernoulli beam theory. These findings will e used in future fatigue experiments as the previous experiment failed do to buckling and due to reaching the machine's deformation limit and as well the load capacity.

Online license transfer

All authors are required to complete the Procedia exclusive license transfer agreement before the article can be published, which they can do online. This transfer agreement enables Elsevier to protect the copyrighted material for the authors, but does not relinquish the authors' proprietary rights. The copyright transfer covers the exclusive rights to reproduce and distribute the article, including reprints, photographic reproductions, microfilm or any other reproductions of similar nature and translations. Authors are responsible for obtaining from the copyright holder, the permission to reproduce any figures for which copyright exists.

Acknowledgements

This paper has been created with the financial support of Czech Science Foundation by project No.: 20−00761S "Influence of material properties of stainless steels on reliability of bridge structures" and by the Brno University of Technology internal grant no: FAST-J-21-7340.

References

S. M. Daghash, Q. D. Huang, and O. E. Ozbulut, 2019. Tensile Behavior and Cost-Efficiency Evaluation of ASTM A1010 Steel for Bridge Construction. "*Journal of Bridge Engineering*". vol. 24, no. 8, Art no. 04019078, doi: 10.1061/(asce)be.1943-5592.0001449.

Ansys, Inc. (2018) ANSYS 19.0. Canonsburg, PA 15317 U.S.A.

Hill, H.N. 1994. Determination of stress-strain relations from the offset yield strength values. Technical Note No. 927. National Advisory Committee for Aeronautics, Washington D.C.

Jindra, D., Kala, Z., Seitl, S., Kala, J., 2020. Material model parameter identification of stainless steel (AISI 304L). Proceedings of 26th International Conference Engineering Mechanics 2020, Brno, Czech Republic, 24.-25.11.2020. ISSN: 1805-8248. ISBN: 978-80-214-5896-3.

Jindra, D., Kala, Z., Kala, J., Seitl, S., 2021. Experimental and Numerical simulation of a Three Point Bending Test of a Stainless Steel Beam, 14th International scientific conference on sustainable, modern and safe transportProcedia Engineering.

Ramberg, W., Osgood, W.R., 1943. Description of stress-strain curves by three parameters. Technical Note No. 902. National Advisory Committee for Aeronautics, Washington D.C.

Mirambell, E., Real, E., 2000 On the calculation of deflections in structural stainless steel beams: an experimental and numerical investigation. Journal of Constructional Research vol.54 p.109-133.